Supporting Information

A Catch and Anchor Approach to Combat both Toxicity and Longevity of Botulinum Toxin A

Lucy Lin[‡, §], Margaret E. Olson[†,‡§], Takashi Sugane[†,‡], Lewis D. Turner[§], Margarita A. Tararina[¶], Alexander L. Nielsen[§], Elbek K. Kurbanov[†,¤], Sabine Pellett[⊥], Eric A. Johnson[⊥], Seth M. Cohen[¤], Karen N. Allen[‖] and Kim D. Janda[,§]*

[§] Departments of Chemistry and Immunology, The Skaggs Institute for Chemical Biology, Worm Institute of Research and Medicine (WIRM), The Scripps Research Institute, 10550 North Torrey Pines Road, La Jolla, California 92037, United States

[‖] Department of Chemistry, Boston University, 590 Commonwealth Avenue, Boston, Massachusetts 02215, United States

[¶] Program in Biomolecular Pharmacology, Boston University School of Medicine, 72 East Concord Street, Boston, Massachusetts 02118, United States

[¤] Department of Chemistry and Biochemistry, University of California San Diego, 9500 Gilman Drive, La Jolla, California 92093, United States.

[⊥] Department of Bacteriology, University of Wisconsin, 1550 Linden Drive, Madison, Wisconsin 53706, United States

[‡] These authors contributed equally

*Corresponding author: kdjanda@scripps.edu

Table of Contents

Additional discussion regarding 3rd generation crystal structures

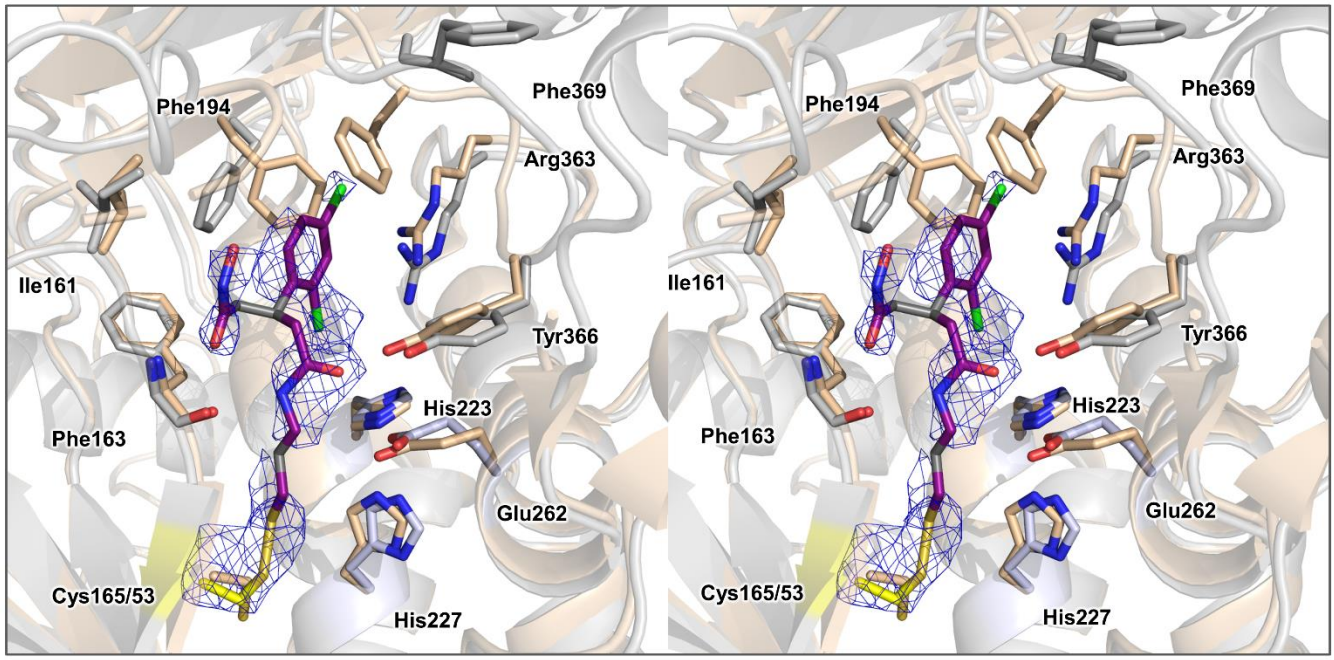

Figure S1. Wall-eyed stereoview of the superposition of BoNT/A LC in complex with **53** (grey cartoon) and with **7** (beige cartoon, PDB 2IMA). The Cys165/**53** adduct is depicted as dark purple sticks with grey atoms corresponding to regions of poor electron density. Cys165 is depicted in yellow. Residues constituting the Zn^{2+}-binding domain are shown in light blue for BoNT/A LC/**53**. The Polder omit map is shown as blue mesh contoured at 3.5σ.

An X-ray crystal structure of **53** in complex with BoNT/A LC was resolved to 2.5 Å resolution. The inhibitor complex was co-crystallized as described for complexes **20**–**22**, phases calculated using molecular replacement with PDB 2IMA as search model (RMSD 0.45 Å), and refined to convergence. Notably, the inhibitor bound with partial occupancy, as some portions of **53** had poor electron density (Figure S1). The final model offered an intriguing result. As designed, **53** would bind in the BoNT/A active site with the 2,4-dichlorophenyl moiety filling the small, hydrophobic pocket defined by loop 370. The three-carbon MTS-containing linker would be appropriately oriented towards Cys165, and the two species would form the inhibitory disulfide bond. However, the structure shows that inhibitor is flipped so that the hydroxamate is oriented away from the Zn^{2+}-binding motif (HEXXH). Instead, the amide linker between the ZBG and electrophile forms hydrogen bonds with the zinc-coordinating residues. Unexpectedly, electron density corresponding to the zinc atom was not present in the active site, although zinc was present in the crystallization milieu. However, the concentration of zinc added may not have been sufficient to overcome the chelating effects of EDTA in the protein buffer. In place of zinc, the carboxyl group of Glu262 shifts to coordinate the two histidine residues, along with the carbonyl and the amine groups of the inhibitor. The absence of the metal and outwards positioning of the hydroxamic acid results in the burying of the 2,4-dichlorophenyl group deep inside the hydrophobic pocket. The plasticity of the active site is clearly observed as this results in a 90° flip of Phe194, introducing pi-pi stacking interactions between the phenyl group and the dichlorophenyl group of **53**, and rotation of the 370 loop, resulting in an 8.0 Å repositioning of Phe369 away from the active site

(Figure S1). This unique orientation in the crystal structure is consistent with the inhibition kinetics, showing decreased potency of the 3rd generation inhibitors compared to the 2nd generation.

The X-ray crystal structure of BoNT/A LC bound with **59** was determined to 1.67 Å resolution and phases calculated by molecular replacement (PDB 3BON; RMSD 0.45 Å). As in the structures described above, the structure of the complex with **59** shows that the inhibitor hydroxamate moiety coordinates the zinc metal in a bidentate fashion (Figure S2A). Compared with the binding of **7**, the dichlorophenyl moiety is rotated 43.9 ° and is coordinated through interactions with Arg363 and Phe194. The 370 loop rotates such that Asp370 is flipped inwards and Phe369 flips outwards from the active site. Notably, the alkyl chain of **59** fits into a hydrophobic pocket lined by Ile161, Phe163 and Phe194, resulting in a rotation of the phenyl ring of Phe194 (Figure S2B).

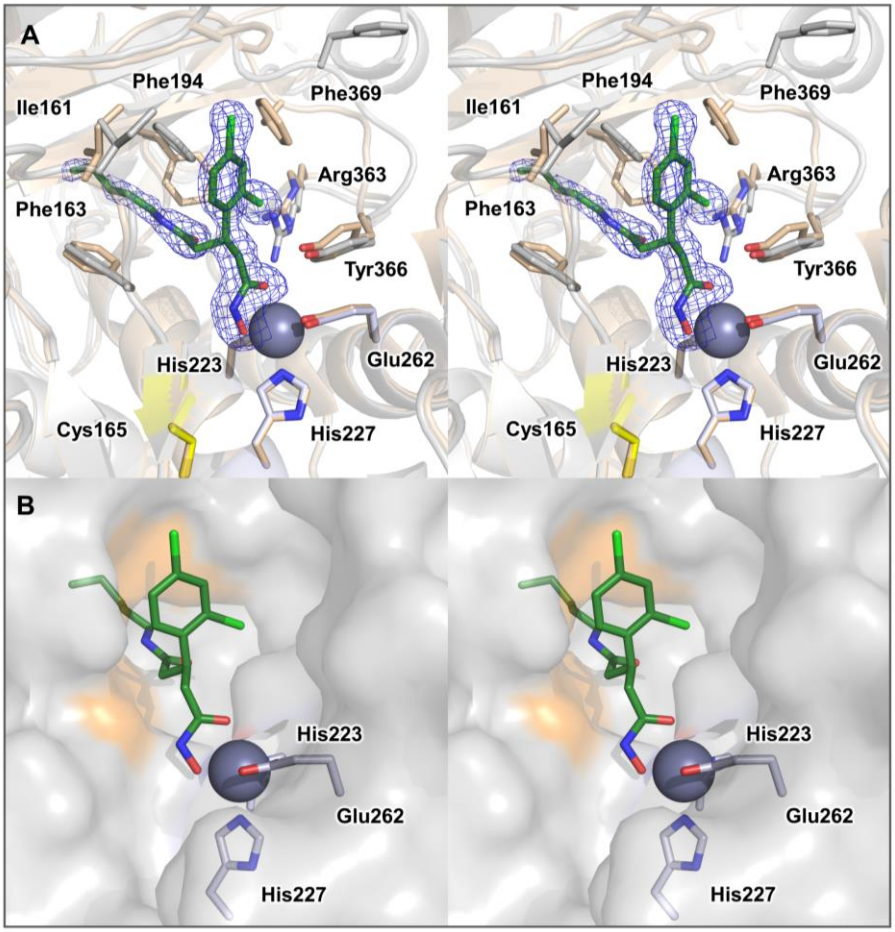

Figure S2. Wall-eyed stereoview of the overlay of BoNT/A LC in complex with **59** (grey cartoon) and **7** (beige cartoon, PDB 2IMA). Cys165 is depicted in yellow, and the Zn^{2+} metal is shown as a purple sphere. Residues constituting the Zn^{2+}-binding domain are shown in light blue for BoNT/A LC/**59**. The Polder omit map is shown as blue mesh contoured at 4.0σ. (**B**) Surface view of **59** with the hydrophobic pocket binding the aliphatic chain highlighted in orange.

Table S1. Components of co-crystallization drops*

Inhibitor solution	**Metal (in ddH_2O)**	**Protein concentration**
20 (4 mM) in 8% DMSO	$Zn(OAc)_2$ (100 mM)	6 mg/ml
21 (2 mM) in 20% DMSO, 80% SM3**	$ZnSO_4$ (10 mM)	6 mg/ml
22 (2 mM) in 20% DMSO, 50% acetonitrile	$ZnSO_4$ (10 mM)	8.6 mg/ml
53 (5 mM) in 10% DMSO, 90% methanol	$ZnCl_2$ (10 mM)	7.2 mg/ml
59 (5 mM) in 10% DMSO, 90% methanol	$ZnCl_2$ (10 mM)	7.2 mg/ml

*All concentrations are final working concentrations prior to addition to the crystallization drop.
***SM3: 25% each of diethylene glycol, glycerol, ethylene glycol, 1,4-dioxane (Molecular Dimensions)

Table S2. Data collection and refinement statistics for X-ray co-crystal structures.

Data collection	BoNT/A LC/**20** (PDB 6XCB)	BoNT/A LC/**21** (PDB 6XCC)	BoNT/A LC/**22** (PDB 6XCD)	BoNT/A LC/**53** (PDB 6XCE)	BoNT/A LC/**59** (PDB 6XCF)
Source	BNL	BNL	BNL	MIT	SSRL
Detector	AMX 17-ID-1	AMX 17-ID-1	AMX 17-ID-1	Bruker APEX2	9-2
Space group	$P2_1$	$P2_1$	$P2_1$	$P2_1$	$P2_1$
Cell dimensions					
a, *b*, *c* (Å)	47.9, 67.3, 63.7	50.4, 66.7, 64.9	50.8, 66.9, 65.1	50.1, 66.5,65.1	49.3, 66.2, 64.1
(°)	97.4	98.6	98.4	98.4	98.5
Wavelength	0.9795	0.91989	0.91989	1.54178	0.97946
Resolution (Å)	1.74 (1.78–1.74)	1.90 (1.94–1.90)	1.92 (1.97–1.92)	2.50 (2.59–2.50)	1.68 (1.70–1.68)
No. of total/ unique reflections	275,187/41,264	110,373/32,771	106,709/32,091	97,143/14,436	153,346/45,292
Completeness (%)	99.5 (94.6)	96.8 (77.7)	97.3 (77.5)	95.3 (83.1)	96.4 (58.2)
$I/\sigma(I)$	10.2 (2.2)	8.4 (1.4)	7.5 (1.3)	7.1 (1.6)	14.1 (1.4)
R_{merge}(%)	10.5 (49.4)	7.3 (76.7)	7.2 (59.7)	20.4 (57.8)	4.6 (56.7)
$CC_{1/2}$	0.99 (0.88)	0.99 (0.69)	0.99 (0.86)	0.96 (0.74)	0.99 (0.78)
Refinement					
Resolution (Å)	28.60–1.74	29.59–1.90	29.68–1.92	29.55–2.50	36.29–1.68
Reflections used in refinement	41,225 (2,667)	32,722 (1,724)	32,009 (1,721)	14,154 (1,110)	45,193 (2,140)
Reflections used for R_{free}	2,000 (136)	1,999 (114)	1,993 (115)	1,417 (123)	1,998 (98)
R_{work} / R_{free} (%)	16.4/20.2 (22.3/26.1)	18.9/23.5 (34.8/39.7)	22.5/27.6 (38.7/45.3)	25.7/31.0 (26.9/35.6)	15.9/19.9 (28.0/28.8)
No. of atoms					
Protein	3,359	3,433	3,427	3,427	3,377
Inhibitor	11	10	12	22	24
Water	293	211	128	55	298
B factors (Å^2)					
Protein	28.8	46.4	54.7	34.6	31.5
Inhibitor	39.8	49.7	56.5	44.0	34.8
Water	37.3	45.4	49.1	30.9	37.7
R.m.s. deviation					
Bond lengths (Å)	0.013	0.007	0.002	0.003	0.016
Bond angles (°)	1.13	0.83	0.48	0.55	1.28
Ramachandran plot (%)					
Most favored	97.5	97.1	96.4	95.1	97.3
Allowed	2.5	2.6	3.1	4.0	2.4
Disallowed	0	0.2	0.5	0.9	0.2

*Statistics for the highest resolution shell are shown in parenthesis

Figure S3. Accompanying images of X-ray crystal structures.

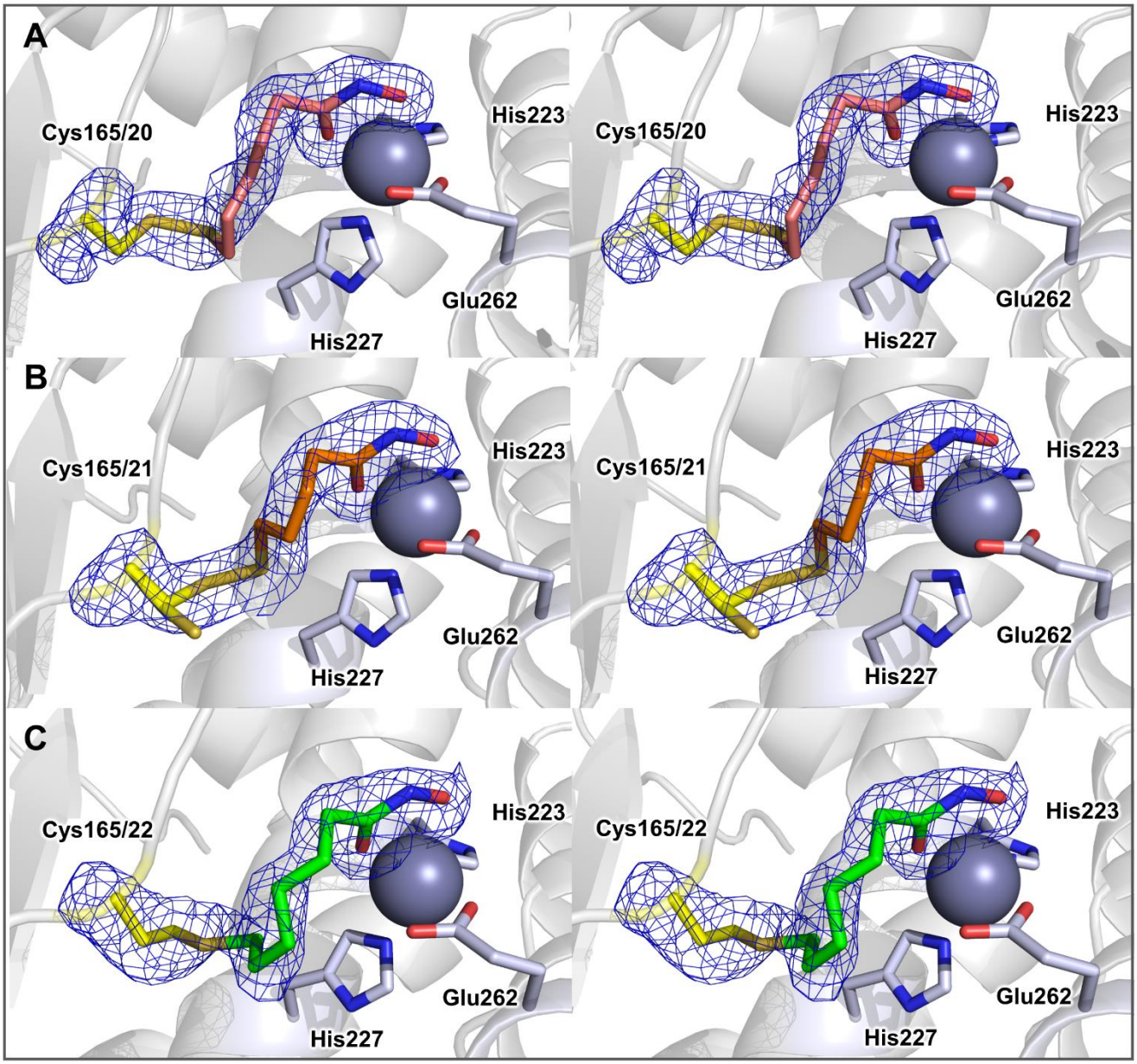

Stereoview of Polder omit maps (blue mesh) contoured at 4.5 σ for compounds (A) **20** in salmon, (B) **21** in orange, and (C) **22** in green bound through covalent attachment to Cys165 of BoNT/A LC. For the BoNT/A LC/**21** complex, two rotamers are shown for Cys165, each with 0.5 occupancy. The Zn^{2+}-binding residues are colored light blue and Zn^{2+} is shown as a purple sphere.

Figure S4. Accompanying images of covalent docking of **31**–**33** and **37**.

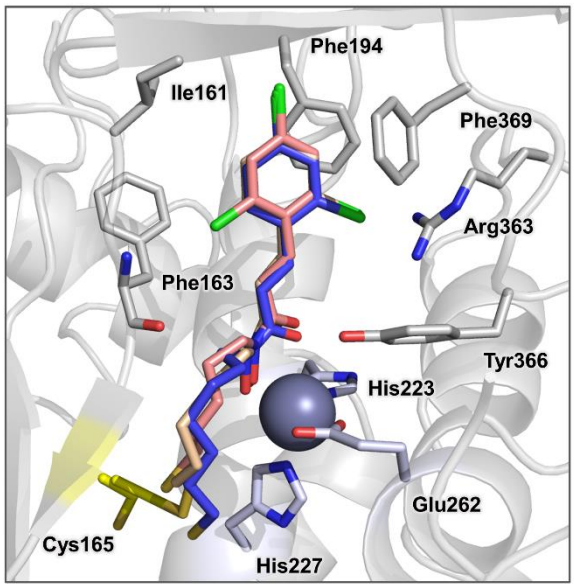

Superposition of the best docking poses of **31** (pink), **32** (wheat) and **33** (blue) covalently docked into the BoNT/A LC active site (PDB 2IMA). The catalytic Zn^{2+} metal is rendered as a purple sphere and Zn^{2+}-coordinating residues are colored light blue. The covalently-adducted, Cys165, is colored yellow. For clarity, only the covalently modified Cys165 of **32** is shown. Respective docking scores are listed below.

Compound	n	Docking score (kcal/mol)
31	5	-7.87
32	6	-8.01
33	7	-7.93

Figure S5. Enzyme models of covalent inhibitors in the presence of substrate.

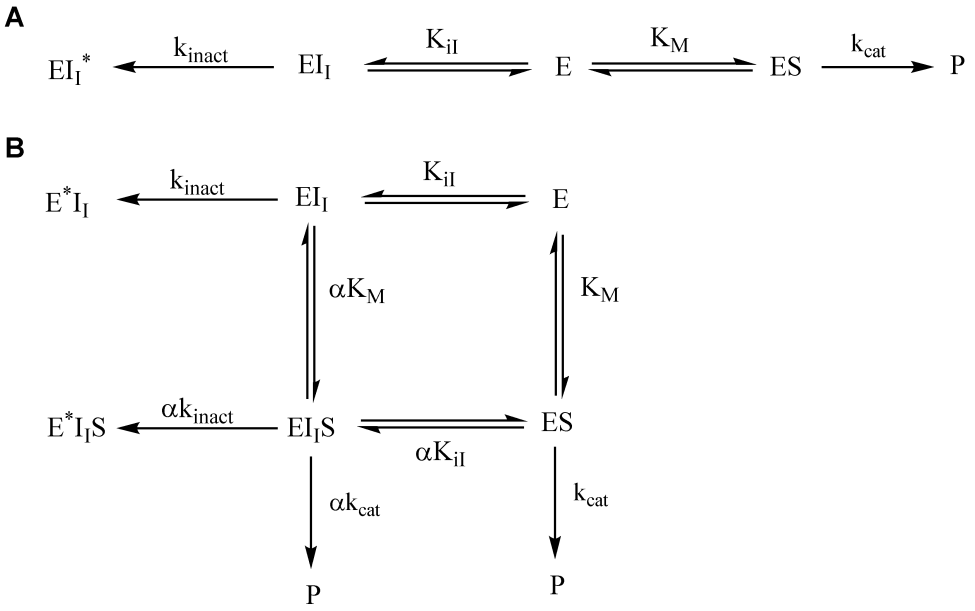

(**A**) Complete covalent inhibitor and enzyme in the presence of substrate. (**B**) Partial covalent inhibitor and enzyme in the presence of substrate.

Figure S6. Statistical comparison of complete and partial models for MTSPA (**4**).

A

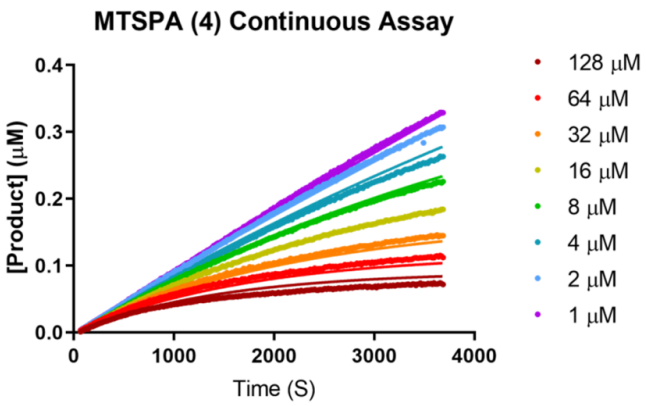

B

	Complete Inhibition	Partial Inhibition
Degrees of Freedom	5781	5780
R^2	0.9716	0.9902
Sum of Squares	0.9402	0.3230
Sy.x	0.01275	0.007475

C

Comparison of Fits	
Null hypothesis	Time Dependent (Competitive)
Alternative hypothesis	Time Dependent (Partial)
P value	<0.0001
Conclusion (alpha = 0.05)	Reject null hypothesis
Preferred model	Time Dependent (Partial)
F (DFn, DFd)	11044 (1, 5780)

(**A**) BoNT/A LC activity in the presence of 4, fit to Equation 2 (partial covalent inhibition). (**B**) Summary of goodness of fit data for Equation 1 (complete inhibition) and Equation 2 (partial inhibition). (**C**) Summary of comparison of fits (extra sum-of-squares) between Equation 1 and 2.

Figure S7. Covalent adduct formation as measured by mass spectrometry.

Compound	Calcd MW	Reacted MW	WT HRMS	WT Difference	WT n	C165S HRMS	C165S Difference	C165S n
None	--	--	50719	--	--	50703	--	--
32	425.03	346.04	51412	693	2	51050	347	1
37	409.03	330.05	51380	661	2	51034	331	1
38	347.05	346.05	50720	1	0	50703	0	0
53	442.02	363.03	51446	727	2	51066	363	1

Figure S8. BoNT/A LC C165S inhibition by **32**, **38,** and **53**.

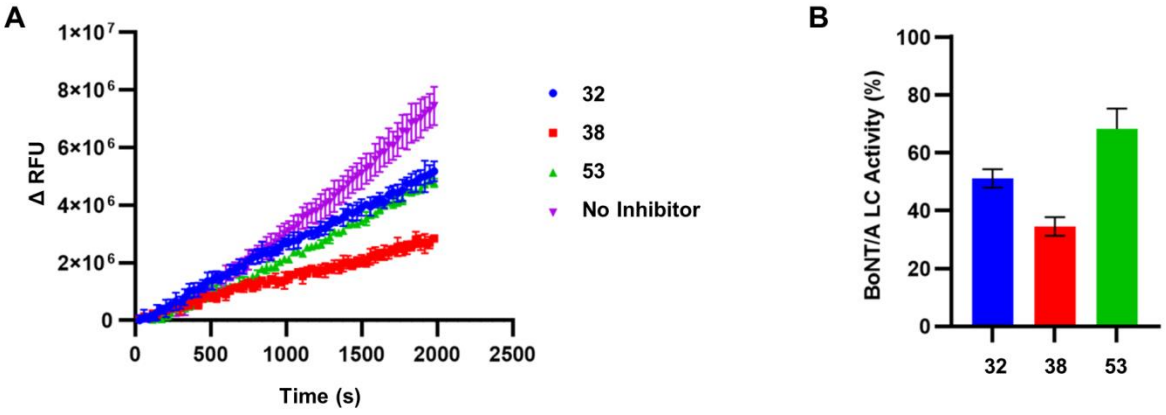

(**A**) Enzyme activity (fluorescence) as a function of time. Fluorescence increases linearly, which is indicative of reversible inhibition. (**B**) Activity of BoNT/A LC mutant C165S after inhibition by compounds at 100 μM. Error bars represent standard deviation (n = 3).

Figure S9. BoNT/A LC inhibition by control compounds **38**, **57**, and **59**.

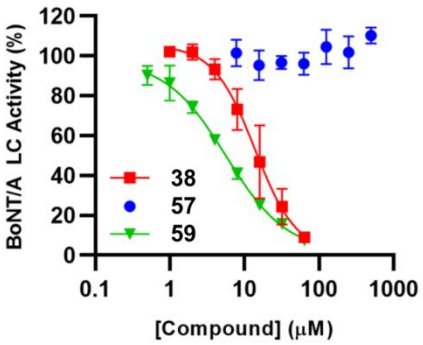

Inhibition of BoNT/A LC WT by compounds **38** (IC_{50} = 14 ± 2 μM), **57**, and **59** (IC_{50} = 5.7 ± 0.6 μM). Error bars represent standard deviation (n = 3).

Figure S10. MMP Activity in the presence of **32** and **53** at 25 μM.

	% Activity Remaining	
MMP	**32**	**53**
MMP-1	16 ± 1	63 ± 4
MMP-2	30 ± 6	84 ± 5
MMP-3	19 ± 3	86 ± 12
MMP-7	11 ± 1	109 ± 9
MMP-8	24 ± 5	79 ± 8
MMP-9	51 ± 0	71 ± 3
MMP-12	21 ± 3	64 ± 10
MMP-13	32 ± 9	69 ± 9
MMP-14	16 ± 0	95 ± 15
MMP-19	35 ± 3	86 ± 19

Activity is expressed as a percentage ± standard deviation (n = 3) of MMP activity in the presence of DMSO control.

Figure S11. SDS-PAGE of expressed BoNT/A LC WT and C165S

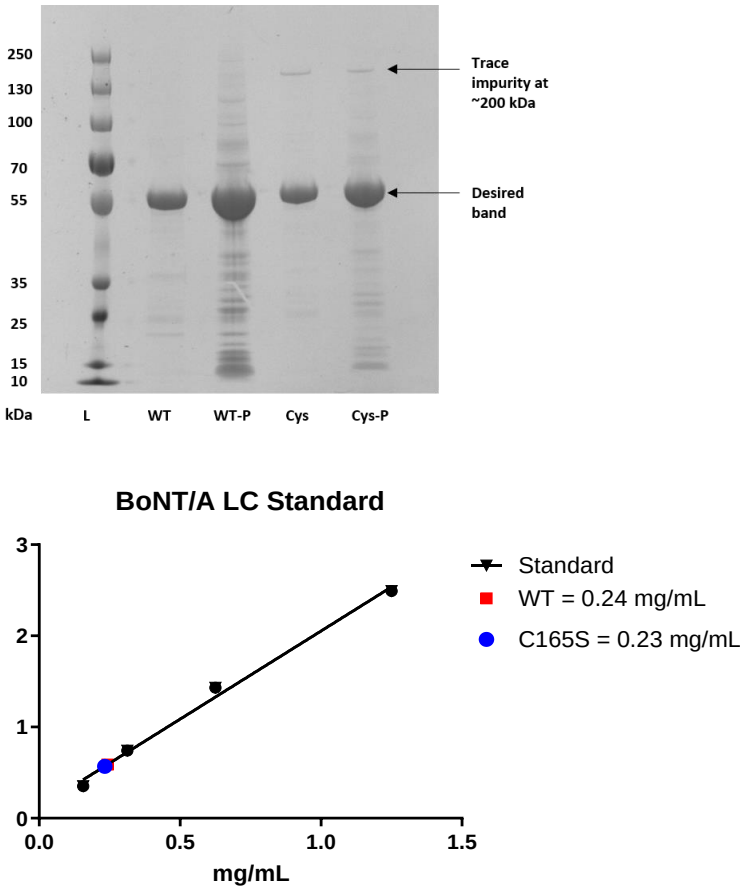

(**A**) SDS-PAGE of purified WT and C165S mutant. L = ladder, P = dialysis precipitate, Cys = C165S mutant. (**B**) Calibration graph to determine concentration of expressed BoNT/A. The BoNT/A standard was provided by William H. Tepp (University of Wisconsin-Madison) at a concentration of 10 mg/mL.

Figure S12. Full images of Western blots for 2nd and 3rd generation bifunctionals

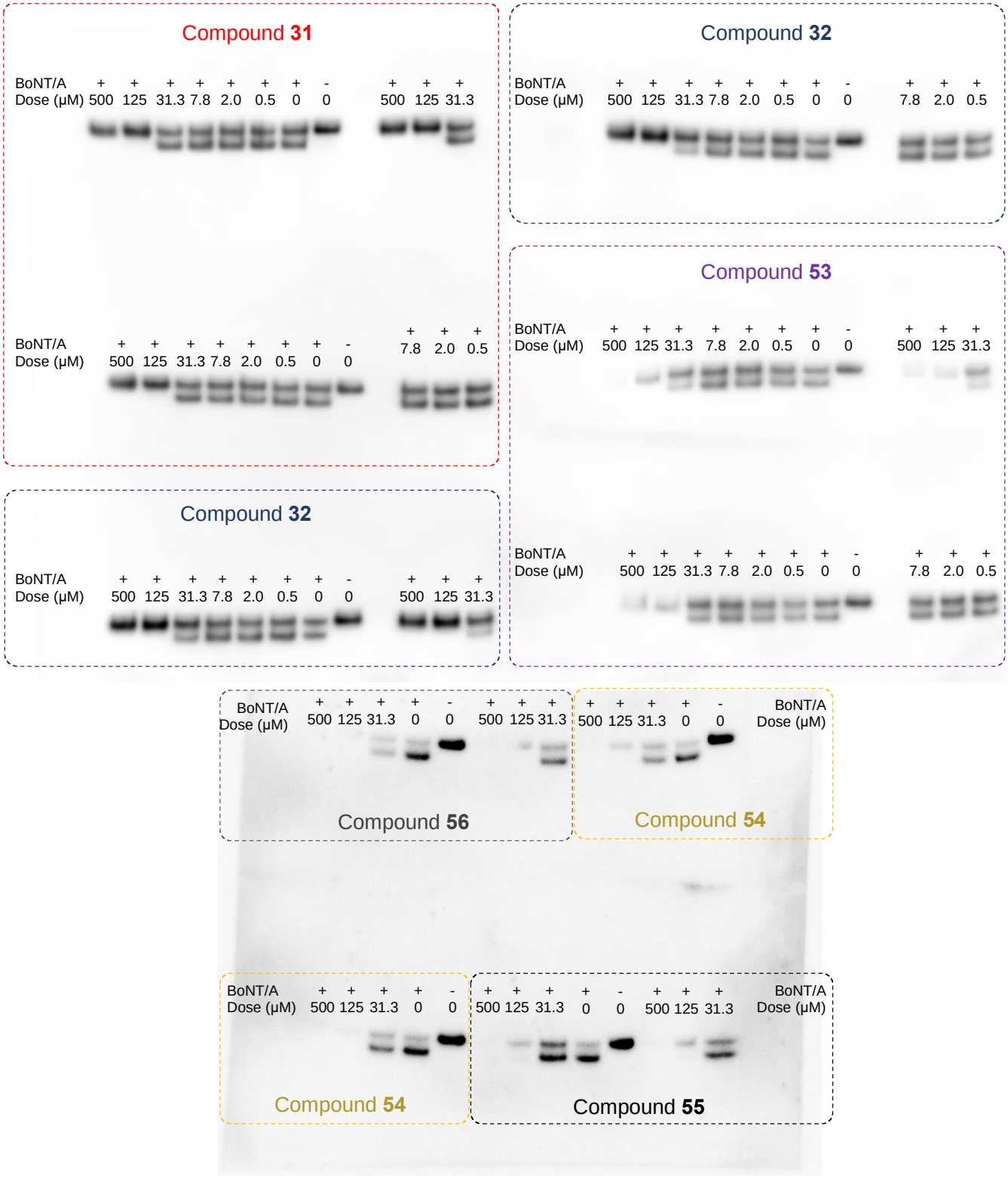

Figure S13. Cell viability results for 3rd generation compounds **54** and **55**

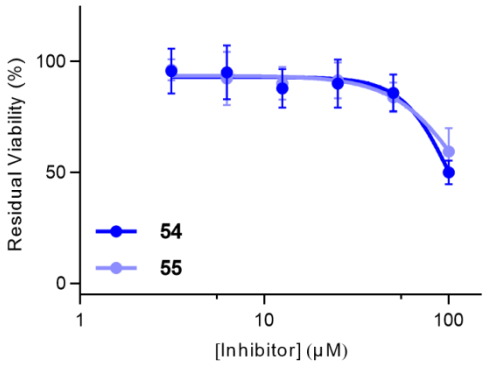

54 (IC_{50} = 128 ± 14 μM) and **55** (IC_{50} = 105 ± 6 μM) were tested in triplicate, simultaneously with **31**, **32**, **53**, and **59**.

Analytical HPLC chromatograms of final compounds

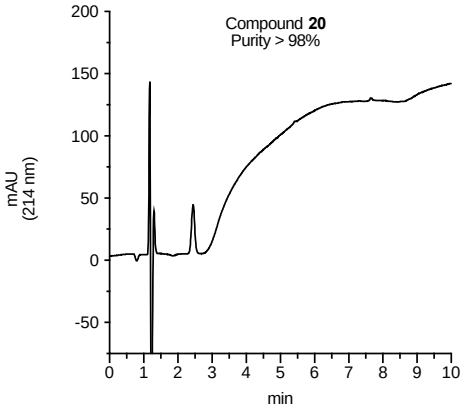

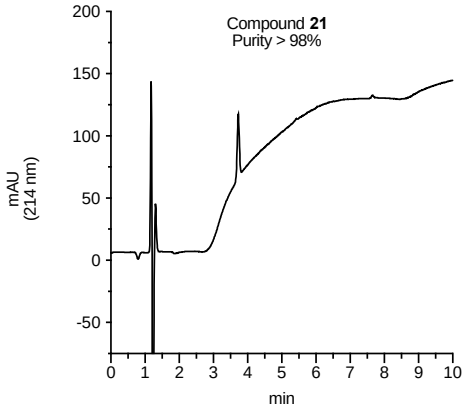

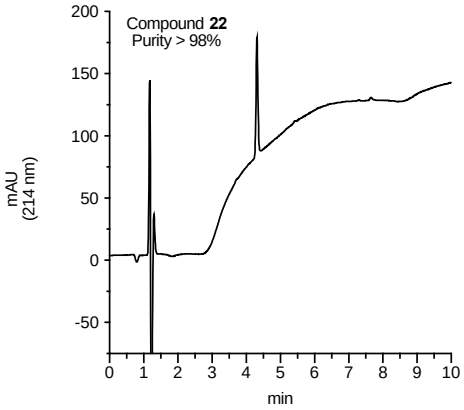

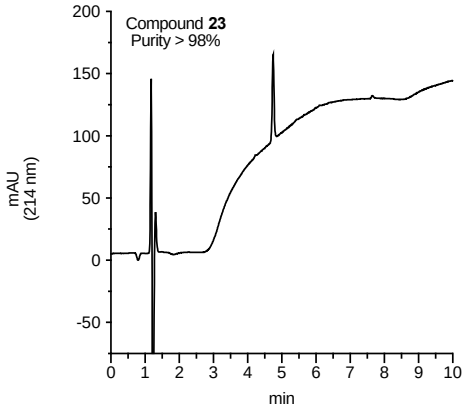

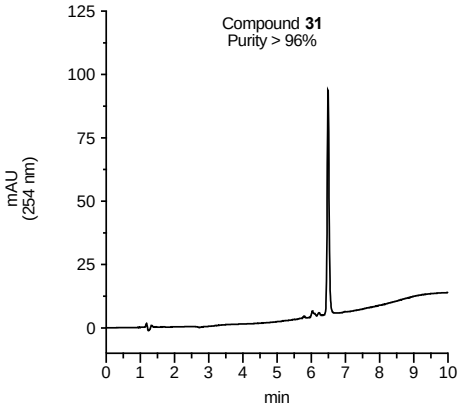

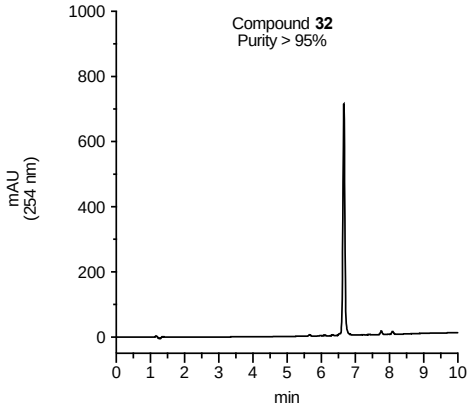

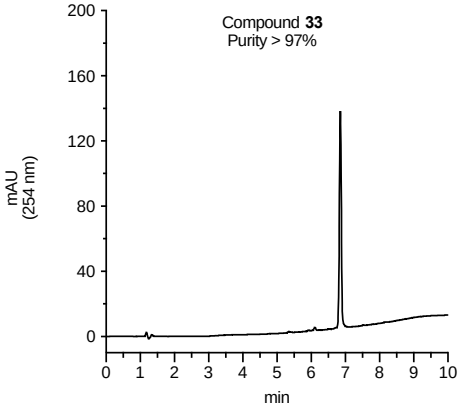

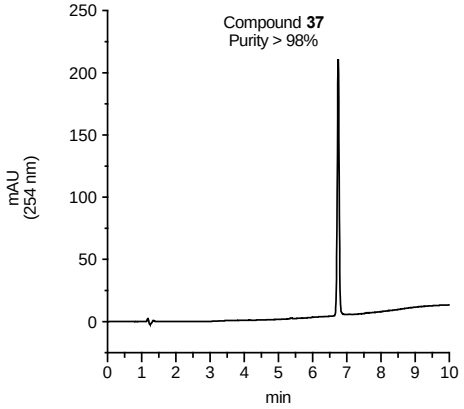

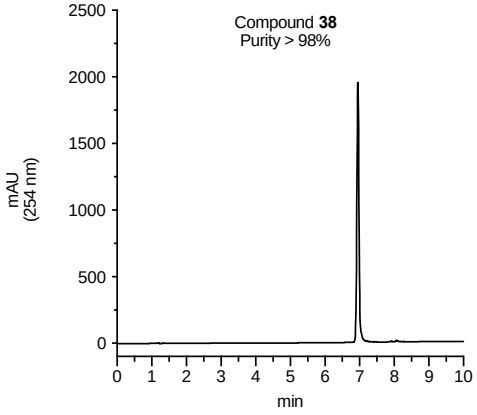
Compound **38**
Purity > 98%
mAU
(254 nm)
min

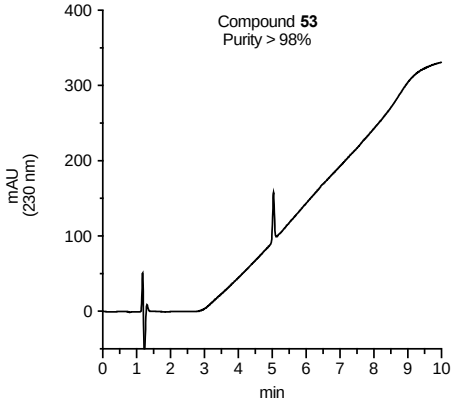
Compound **53**
Purity > 98%
mAU
(230 nm)
min

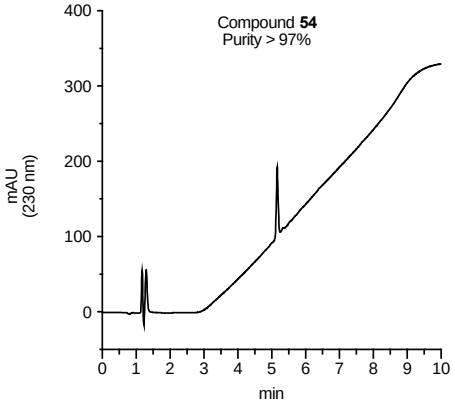
Compound **54**
Purity > 97%
mAU
(230 nm)
min

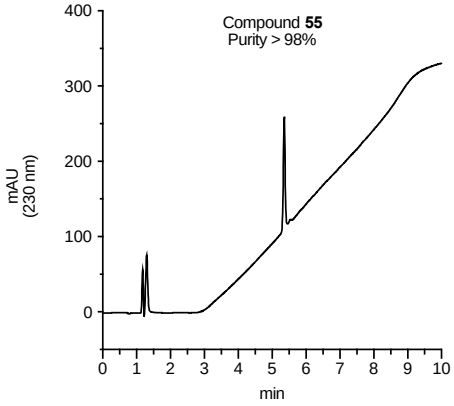
Compound **55**
Purity > 98%
mAU
(230 nm)
min

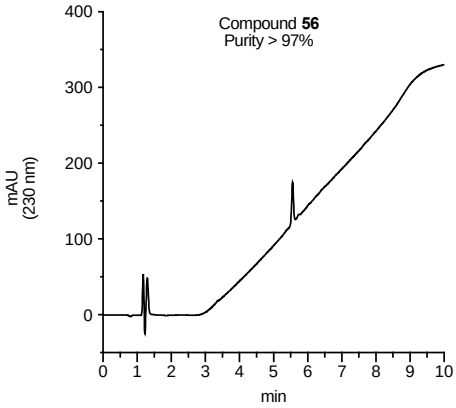
Compound **56**
Purity > 97%
mAU
(230 nm)
min

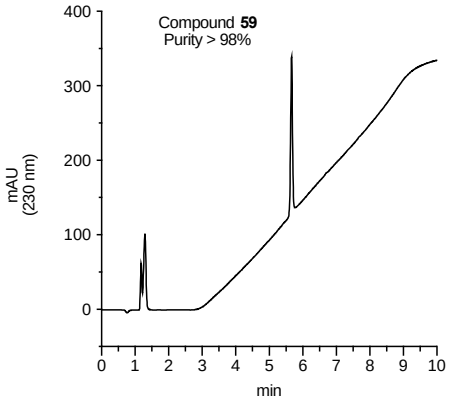
Compound **59**
Purity > 98%
mAU
(230 nm)
min